CORA Cork Open Research Archive
Cartlann Taighde Oscailte Chorcaí

Title	Size dependent thermal properties of embedded crystalline germanium nanowires
Authors	Audoit, Guillaume;Kulkarni, Jaideep S.;Morris, Michael A.;Holmes, Justin D.
Publication date	2007-01-31
Original Citation	Audoit, G., Kulkarni, J. S., Morris, M. A. and Holmes, J. D. (2007) 'Size dependent thermal properties of embedded crystalline germanium nanowires', Journal of Materials Chemistry, 17(16), pp. 1608-1613. doi: 10.1039/B616216A
Type of publication	Article (peer-reviewed)
Link to publisher's version	https://pubs.rsc.org/en/content/articlepdf/2007/jm/b616216a - 10.1039/B616216A
Rights	© The Royal Society of Chemistry 2007
Download date	2026-09-16 18:39:33
Item downloaded from	https://hdl.handle.net/10468/8141

UCC
University College Cork, Ireland
Coláiste na hOllscoile Corcaigh

Size Dependant Thermal Properties of Embedded Crystalline Germanium Nanowires

Guillaume Audoit, Jaideep S. Kulkarni, Michael A. Morris and Justin D. Holmes*

Department of Chemistry, Materials Section and Supercritical Fluid Centre, University College Cork, Cork, Ireland.

**To whom correspondence should be addressed: Tel: +353 (0)21 4903608; Fax +353 (0)21 4274097; E-mail: j.holmes@ucc.ie*

Abstract

Here we report the size-dependence melting points of crystalline germanium nanowires confined within the pores of hexagonal mesoporous silica templates. A supercritical fluid deposition technique was used to form the nanowire-template composite materials and differential thermal analysis, coupled to thermal gravimetric analysis, was used to determine the melting points of the embedded Ge nanowires with mean diameters ranging from 22 to 85 Å. The melting points of the Ge nanowires within the templates were found to be higher than the melting point of bulk germanium (937 °C), typically by 60 °C, and with a broad melting range (~80 °C). Extended X-ray absorption fine structure (EXAFS) analysis of the Ge k-edge from the nanocomposite materials revealed a linear increase in the Ge-Ge nearest neighbour distance with decreasing nanowire diameter over the size range investigated. In all cases the Ge-Ge first shell distance in the nanowires was greater than in the bulk. This observed lattice expansion can be attributed to

crystallographic deformation resulting from the strain imposed on the nanowires by the template. EXAFS studies also revealed an increase in the average number of oxygen atoms at the Ge/silica interface with decreasing diameter, which is due to the increasing surface area with decreasing nanowire diameter. Interfacial effects and interactions at the nanowires/matrix interface are believed to delay the melting point of these systems.

Introduction

One-dimensional structures, such as nanowires and nanotubes, are potential candidates as nanoscale building blocks for the next generation of electronic and photonic devices due to their unique size-dependent properties. In particular semiconductor nanowires such as silicon and germanium have been the focus of much research because of their compatibility with current CMOS processing in the microelectronics industry [1]. Si and Ge nanowires have been synthesised using a wide range of synthetic methods including chemical vapour deposition (CVD) [2-6], arc-discharge [7], sol-gel processing [8], molecular beam epitaxy [9] and supercritical fluid (SCF) routes [1, 10-13]. SCFs are excellent solvents for impregnating these materials into porous templates due to their excellent penetrating powers minimising pore blocking [14]. Our group has developed SCF techniques for producing high density arrays of ordered nanowires and nanotubes within porous template such as mesoporous silica and alumina membranes [15, 16]. Templated synthesis is an extremely effective way of providing size-monodispersed nanowires of different aspect ratios [17] which is critical for measuring size-dependent properties, such as photoluminescence emission [11]. Moreover, the integration of nanowires within real devices will require them to be assembled and oriented relative to a substrate surface.

The integration of low-dimensional systems into any working device requires a complete examination of their thermal properties to ensure structural and functional integrity and stability over the expected operating temperature range. Pawlow's pioneering work [18] theorised the relationship between the size and the melting point of small particles compare to the bulk, i.e. a melting point depression occurs with decreasing particle size. Theoretical studies have established that the high surface to volume ratio of nano-structured materials such as clusters [19, 20], nanodots [21-23]and nanowires [24-26](compared to macroscopic systems) results in a depression of the melting point. Experimental data has also shown the depression of the melting point for gold [27], indium [28], tin [29] and silver [30] nanoparticles and germanium nanowires within carbon nanotubes [31] is attributed to the high number of loosely bound surface atoms which possess a lower cohesive energy than the atoms within the bulk. However, in some cases an increase of the melting point for nanoparticles is observed with decreasing diameter. This phenomenon is called superheating [32]. Nanocrystals coated by or embedded in a matrix of a different material, with a higher melting temperature, exhibit elevated melting points compared to the related bulk material. There are reports of superheating for a number of systems such as In [33, 34] and Pb [35] nanoparticles embedded in an Al matrix, Pb nanoparticles in Zn [36], and Ag nanoparticles in Ni [37]. Recently Wang et al have reported the size dependant melting behaviour of Zn nanowires within AAO membranes [38]. In this paper we report on the use of Extended X-ray Absorption Fine Structure (EXAFS) spectroscopy to probe the superheating properties of Ge nanowires, with mean diameters of 22, 50, 60 and 85 Å, encased within hexagonal mesoporous silica (HMS) matrices.

Experimental

Preparation. The synthesis of tunable hexagonal mesoporous silica (HMS) has been comprehensively described in previous work [39]. Briefly, HMS was prepared by the acid hydrolysis of tetramethoxysilane (TMOS) in the presence of a polyethylene oxide (PEO)-polypropylene oxide (PPO)-polyethylene oxide (PEO) triblock copolymer surfactant, P85 ($PEO_{26}PPO_{39}PEO_{26}$) and P123 ($PEO_{20}PPO_{69}PEO_{20}$). The decomposition of TMOS during the hydrolysis generates methanol which is then completely removed using a rotary film evaporator at 40 °C. The resulting gel was then left to condense at 40 °C for one week before being calcined at 450 °C. Smaller diameter HMS was achieved using the surfactant Brij 35 ($C_{12}EO_{23}$). Germanium nanowires were produced within the pores of the HMS using a SCF inclusion-phase technique [11, 40]. In a typical preparation, the HMS was degassed at 200 °C under a flow of nitrogen for 6 hr to remove residual moisture and other pore contaminants. The HMS and the Ge precursor were placed in a high pressure vessel and sealed under a nitrogen atmosphere. The loaded reaction cell was then connected to a high-pressure CO_2 pump, via a 3-way valve and CO_2 solvent reservoir, and placed in a tube furnace at 500 °C and 375 bar for 30 min. The white HMS loaded into the reaction vessel became silvery-black after Ge nanowire inclusion. No colour change was noticed in the absence of the semiconductor precursor. The product was then washed in anhydrous hexane, chloroform and ethanol before being dried for analysis. The HMS-nanowire composite materials are coded as Ge50 etc., i.e. Ge nanowires encased in a HMS matrix with a mean diameter of 50 Å.

Powder X-ray diffraction (PXRD) profiles were recorded on a Philips X'Pert diffractometer, equipped with a Cu-K_α radiation source and X'Celerator detector. Height and reflected stöller

slits of 0.2° were used with a programmable divergent slit to maintain a 10 mm footprint at the sample. Sample heights, were determined at $\theta = 2\theta = 0$ at the point when the sample reduced the beam intensity by 50 %.

N_2 Adsorption Measurements. Surface areas of the calcined HMS were measured on a Micromeritics Gemini 2375 nitrogen adsorption instrument and calculated based upon Brunauer–Emmett–Teller (BET) isotherms. Prior to the adsorption measurements, each sample was degassed for 12 h at 200 °C under a high purity nitrogen flow to remove any residual moisture from within the pores. The surface area and mean pore size distribution of the calcined silicas was calculated based on the Brunauer–Emmett–Teller (BET) and Barrett– Joyner–Halanda (BJH) models respectively. All of the HMS examined exhibited a characteristic type IV adsorption isotherm profile [41]. In all cases, hysterises was observed in the isotherms. Adsorption isotherms were used to calculate the pore diameter distributions.

Melting Point Measurements. The melting temperatures of the dried Ge-HMS nanocomposites were determined using simultaneously Differential Thermal Analysis (DTA) and Thermal Gravimetric Analysis (TGA) measurements (40 mg placed in a Pt crucible) using a Stanton Redcroft STA 1640 (Rheometric Scientific, Epsom, UK) apparatus. Each sample was heated form 100 °C to 1100 °C at a heating rate of 10 °C. min^{-1} under a nitrogen flow (4 $L.hr^{-1}$) to minimize oxidation. The melting region of the crystalline Ge nanowires was determined by giving particular attention to the analysis of endothermic events in the bulk Ge melting region (around 937 °C).

Extended X-ray Absorption Fine Structure (EXAFS) Measurements. EXAFS measurements performed using the 2 GeV synchrotron radiation source at station 16.5 at the CLRC Daresbury Laboratory (Cheshire, UK). The absorption measurements taken on the Ge K-edge (11105 eV) were performed in transmission mode at -196 °C. The incident X-ray beam was monochromatized using a Si (111) double-crystal monochromator. Two ionization chambers, filled with Ar gas, monitored the incident and transmitted X-ray intensities, I_0, and I_t, respectively allowing determination of the linear absorption coefficient (μ). Data are an average of 2 scans. The spectra were calibrated using the Daresbury program EXCALIB, background subtracted and normalized using the program EXPLINE. The data were simulated using k^3-weighted EXAFS employing theoretical phase shifts calculated with Hedin–Lundqvist exchange potentials and von Barth ground states using the program EXCURV98 [42]. The theoretical fits were obtained by adding shells of backscattering atoms around the central Ge absorber atom and refining the Fermi energy (E_f) the absorber–scattered distances (r) and the Debye–Waller factors ($2\sigma^2$) in order to minimize the R-factors (indicating the merit of the fit). The absolute value of the R-factor will depend on noise levels within the data and the data range. For the spectra presented in this paper, R values less than 25 represented a good fit.

Results and Discussion

The mesoporous silicas prepared in this study showed well-resolved peaks characteristic to well-ordered mesoporous structures. Figure 1a shows low angle powder X-ray diffraction (PXRD) patterns for a calcined mesoporous silica templated from the triblock copolymer surfactants P85 before (HMS-P85) and after Ge inclusion (Ge50). Three well resolved peaks can be readily indexed to (100), (110) and (200) reflections for a hexagonal mesoporous solid. The mesoporous

silica template remains hexagonally ordered with no shift of the (100) peak after Ge inclusion. Clearly, the mesoporous silica templates are sufficiently robust to withstand the SCF reaction conditions used in the present experiments. Prior to nanowire inclusion, all the HMS displayed type IV adsorption-desorption isotherms characteristic of mesoporous materials [41] as illustrated in figure 1b for HMS-P85. Figure 1c displays the mean pore size distribution of a HMS–P85 sample before nanowire inclusion. The pore size determined by nitrogen adsorption measurements is an important parameter as it corresponds to the mean diameter of the nanowires synthesised within these pores, namely Ge22 (± 3 Å), Ge50 (± 5 Å), Ge60 (± 5 Å), Ge 85 (± 10 Å). Table 1 lists the physical characteristics of all the HMS matrices and the Ge–nanocomposite materials as determined by N_2 adsorption measurements. All of the HMSs exhibited high surface areas (S_A) which drastically drop after nanowires inclusion. An almost complete filling of the pores is achieved as partly confirmed by the decrease of the pore volume (V).

Figure 2 shows the PXRD pattern of templated Ge nanowires, with a mean diameter of 50 Å (Ge50), after background subtraction. The diffraction peaks correspond to the (111), (220), (311) and (331) planes of the diamond structure of Ge (JCPD number 04-0545) and is characteristic of a highly crystalline Ge-HMS material.

Figure 3a shows the DTA/TGA data from bulk Ge powder. The sharp DTA endothermic peak, (negative) at 937 °C corresponds to the melting point of bulk Ge [43]. The DTA curve shows the temperature at which the melting transition of a material occurs. Figure 3b shows the DTA data obtained from Ge nanowires, with mean diameters of 22, 50, 60 and 85 Å, incorporated within HMS matrices between the temperature range of 500 to 1100 °C (labelled Ge22, Ge50, Ge60 and

Ge85 respectively). Superheating phenomena is observed for Ge60, Ge50 and Ge22 samples with melting points of 1004 °C, 1008 °C and 1046 °C respectively. Hence, the melting point of the nanocomposite materials was observed to increase with decreasing nanowire diameter. The DTA curve of the Ge85 sample, shown in figure 3b, exhibits an endothermic peak in the same region as bulk Ge, i.e. 940 °C, but the DTA profile is completely different compared to the bulk. The DTA peak from Ge85 at 940 °C is significantly broader suggesting the melting point of the nanowire sample takes place over a larger temperature 'window', about 75 °C, compared to bulk Ge where the temperature window is 14 °C. The broadness of the melting point transition is attributed to the broad size distribution of the nanowires. Figure 3c illustrates the melting point for Ge50, which has a melting range over 60 °C. As summarised in table 1, the size distribution is narrow for Ge22 (± 2 Å) and increases progressively with pore diameter, corresponding to a narrower melting window of 40 °C for Ge22 compare to 60 °C for Ge50. Figure 3d illustrates very well that the wider the pore size distribution is, the broader the melting range. The silica template significantly influences the melting point of the Ge nanowires compared to free-standing nanowires, i.e. not held within a matrix, which exhibit a melting point that is lower than the corresponding bulk, as previously predicted for different systems [24-26]. We suggest that the superheating observed with the templated Ge nanowires arises due to binding of the interfaces between the crystalline Ge nanowires and the amorphous silica. Superheating possible occurs because the initial formation of the liquid layer at the surface of the nanowire is physically or energetically hindered by the templating matrix.

EXAFS measurements can provide information on the structural environment of chosen atoms within a matrix. EXAFS studies on the Ge nanowire-silica composite materials was carried out

using the Ge adsorption K-edge, allowing the structural properties of the nanowires and of the Ge-silica interface to be probed in order to understand the observed superheating behaviour. Figure 4 shows the Fourier transform of the Ge K-edge EXAFS spectrum of the Ge nanowires within the mesoporous silica templates with diameters of 22, 50, 60 and 85 Å as well as 2 standards, Ge and GeO_2. Best fit results are summarized in table 2. Two distinct shells can clearly been seen, the first one at a distance around 1.74 Å and the second one at 2.45 Å from the central target Ge atom. The first shell is related to an oxygen environment with a distance corresponding to the usual Ge-O length of 1.74 Å. The shell at 1.74 Å is attributable to Ge bound to oxygen atoms on the walls of the silica matrix. EXAFS features around this value of distance are difficult to quantify and prone to error because they reflect poorly defined features in the raw data. Thus derived co-ordination numbers may reflect the presence of Ge-O bonding but may not imply a large amount of oxidation of the bulk Ge. A peak at 3.1 Å is observed in figure 4 (ii) to (v) which would corresponded to the Ge-Ge distance in a GeO_2 structure (figure 4(i)). This suggests that although the PXRD data doesn't indicate presence of GeO_2 a small amount of GeO_2 may be present. Table 2 lists all the data obtained from the EXAFS measurements. The number of O atoms close to the Ge atoms increases with decreasing nanowire diameter, due to the increasing radii of curvature. As a result there are more O atoms per atom of Ge with decreasing nanowire diameter. As noted above the listed co-ordination values reflect the increasing Ge-O bonds rather than the actual content of bulk oxidation which is too small

For all the Ge nanocomposite materials, the next nearest atoms to Ge are other Ge atoms at a bond distance of around 2.45 Å, corresponding to the distance between two Ge atoms in the

tetrahedral site of a cubic lattice (Ge diamond structure). The distance between the two Ge atoms is seen to increase with decreasing diameter from a bulk-like value, 2.45 Å, for a mean nanowire diameter of 85 Å, to 2.47 Å for a mean nanowire diameter of 22 Å as shown in figure 5a. These data confirm PXRD measurements previously reported [11]. Lattice expansion of the Ge structure has been attributed to the external strain imposed by the surrounding silica matrix on the templated nanowire which prevents any relaxation of the crystal structure compare to its free-standing counterparts. The extent of lattice expansion could be affected by the nature of the template material since the interfacial bonding depends on the nature of the template. Besides the growth methods could also affect the crystal structure of the nanowire and thus its lattice parameters.

The average Ge-Ge co-ordination number decreases with decreasing nanowire diameter, i.e. 2.4 and 1.0 for mean diameters of 85 and 22 Å respectively. This observed decrease is a consequence of the increasing radii of curvature of the nanowires with decreasing dimensions, i.e in smaller nanowires there are more Ge atoms bound to O atoms at the nanowire/matrix interface. The relationship between the average co-ordination number of the first two shells around the Ge atoms and the mean diameters of the nanowires is shown in figure 5b and table 2.

The correlation between the co-ordination number of the surface atoms and the melting point of nanocrystalline materials has been previously investigated by Sun et al. [44]. This work suggested that in the case of an embedded nanomaterial, an increase of the melting point originates from interfacial effects. With our templated nanocomposite materials strong interactions at the interface between the nanowire and the matrix, and the fact that the bond enthalpy between Ge-O and Ge-Ge is significantly larger [45], i.e. 385 $kJ.mol^{-1}$ compared to 188 $kJ.mol^{-1}$ leads to the

observed superheating. Hence, the increasing number of O atoms at the nanowire/matrix interface with decreasing nanowire diameter results in an increased number of Ge-O interactions, which explains why Ge22 melts at a higher temperature than Ge50. It should be noted that for nanowires present within a HMS template the decreasing diameter directly results in an increase in the oxygen content at the interface due to the increase in the ratio of surface/bulk atoms. Hence although the increase in melting point with decreasing diameter of the nanowires can be attributed to increasing oxidation of germanium, the oxidation itself is size dependant.

In summary, we report here the size-dependant superheating of Ge nanowires encased within a mesoporous silica matrix. The nanowire-silica materials were observed to melt up to 109 °C above the melting point of bulk Ge for the smallest nanowires investigated. The superheating observed can be ascribed to the presence of the O atoms at the nanowire / silica interface and more particularly to their strong interaction with the Ge atoms at the surface of the nanowires. The silica walls act like a high energetic shell around the nanowire delaying it from melting at the bulk melting point value. The exact role of the silica wall needs further investigation by etching the nanowires from the template. This experimental work reports the superheating in a matrix/nanowire system and represents valuable information for future nanodevice manufacturing.

Acknowledgements

The authors acknowledge financial support from the Irish Research Council for Science, Engineering and Technology (IRCSET) (Project SC/02/4). The authors would like to thank

Mark Robertson for valuable time related to EXAFS and Dr. David O'Sullivan, Materials Ireland Research Centre, University of Limerick for thermal analysis.

Table 1 Nitrogen Adsorption data for HMS and associated silica/germanium nanocomposites (Surface Area (S_A) and pore Volume (V)).

	Mean Pore Diameter (Å)	Pore size distribution (Å)	Mean Wall thickness (Å)	S_A ($m^2.g^{-1}$)		V ($cm^3.g^{-1}$)	
				HMS	HMS-Ge	HMS	HMS-Ge
Brij 35	22	20-25	18	946	65	0.75	0.02
P 85	50	45-55	25	780	32	0.95	0.04
P123	60	55-65	30	520	36	0.59	0.03
Swelled P123	85	75-95	18	500	23	0.70	0.05

Table 2 EXAFS data of sample sets. Error bars are from the IXS Standards and Criteria Committee. The Ge-O and Ge-Ge interatomic distances have also been measured from bulk GeO_2 and Ge respectively and are equal to 1.742 and 2.453 Å.

	Nanowires Diameter (Å)	22	50	60	85
	Surface / Volume (%)	18.2	8.0	6.7	4.7
1st Shell Ge-O	Interatomic distance (± 0.001 Å)	1.746	1.736	1.732	1.742
	C.N.	2.9	2.3	2.25	1.6
2nd Shell Ge-Ge	C. N.	1.0	1.7	1.71	2.4
	Interatomic distance (± 0.001 Å)	2.473	2.466	2.459	2.456

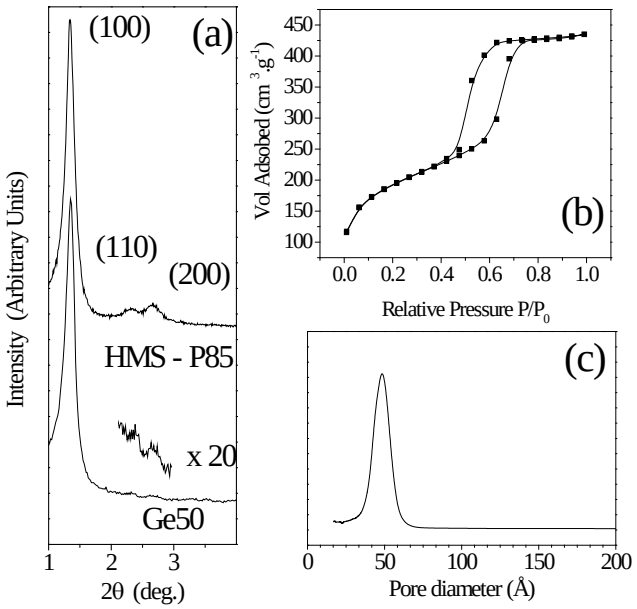

Figure 1 (a) Low angle PXRD of the HMS made from surfactant P85 before (HMS – P85) and after (Ge50) inclusion of Germanium. (b) Nitrogen adsorption hysteresis and (c) pore size distribution of the HMS – P85.

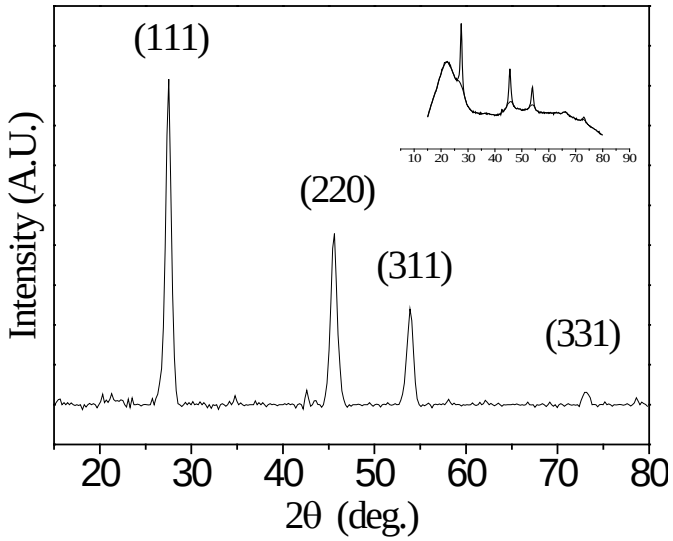

Figure 2 Typical Powder X-Ray diffraction of a Ge composite material (Ge65) after Background subtraction showing the (111), (311), (331) and (422) plane diffraction. Inset shows the corresponding raw data.

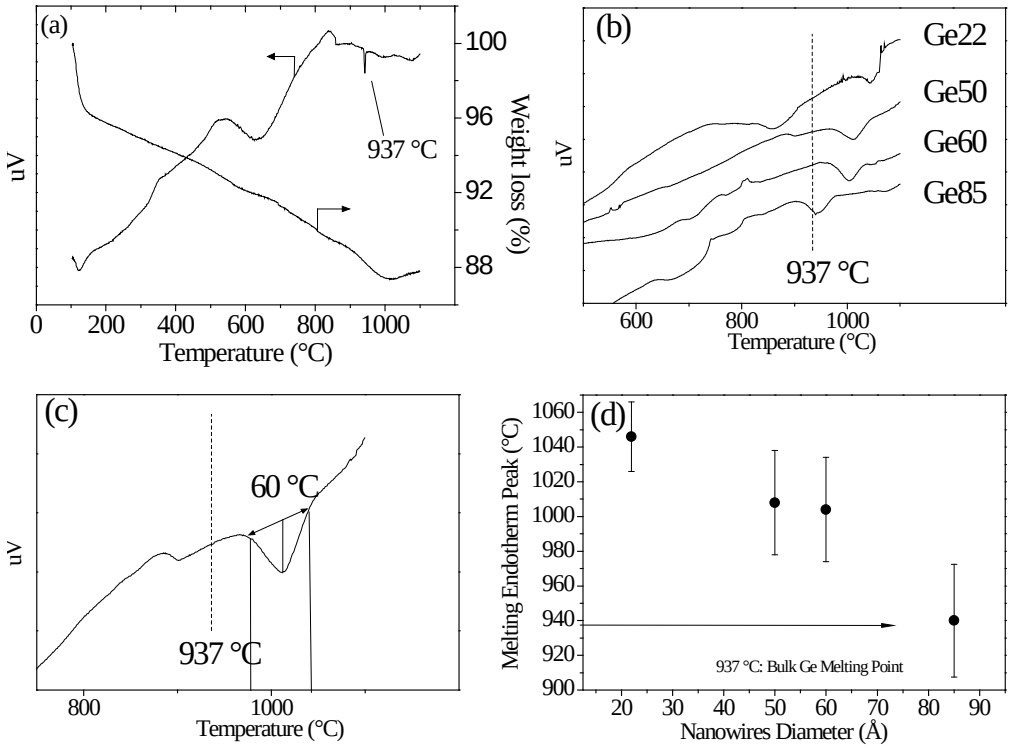

Figure 3 (a) DTA/TGA curves of Bulk Ge standard with a sharp endothermic peak at 937 °C with no mass loss. (b) DTA curves of Ge22, Ge50, Ge60 and Ge85 showing the endothermomic melting phenomena above 937 °C. (c) Detailed view of the Ge NWRs melting region for Ge50 with a peak at 1008 °C and a melting range of 60 °C. (d) Melting point peak position in function of the nanowires diameter, the error bars represent the melting range of Ge within the pores of the HMS.

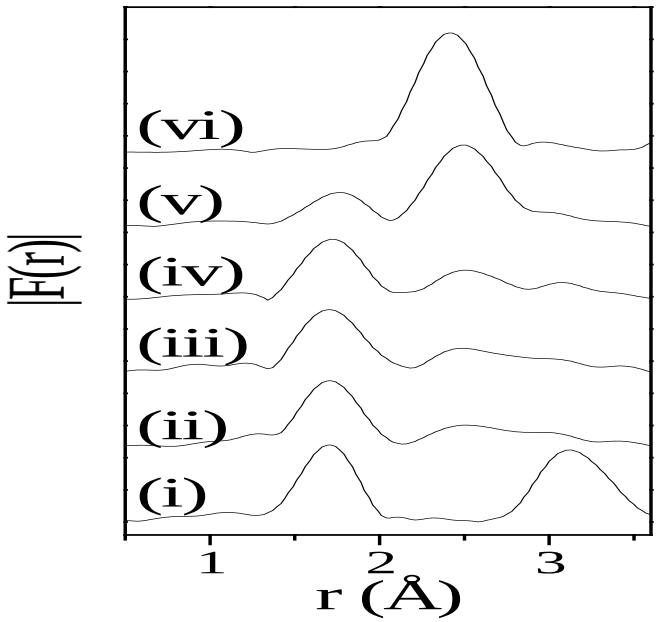

Figure 4 Absolute values of Fourrier transform of $k^3\chi(k)$ into r space, |F(r)|, for Bulk GeO_2 (i), Ge22 (ii), Ge50 (iii), Ge60 (iv), Ge85 (v) and Bulk Ge (vi). First peak near r = 1.74 Å corresponding to Ge-O distance and second near r = 2.45 Å corresponding to Ge-Ge distance.

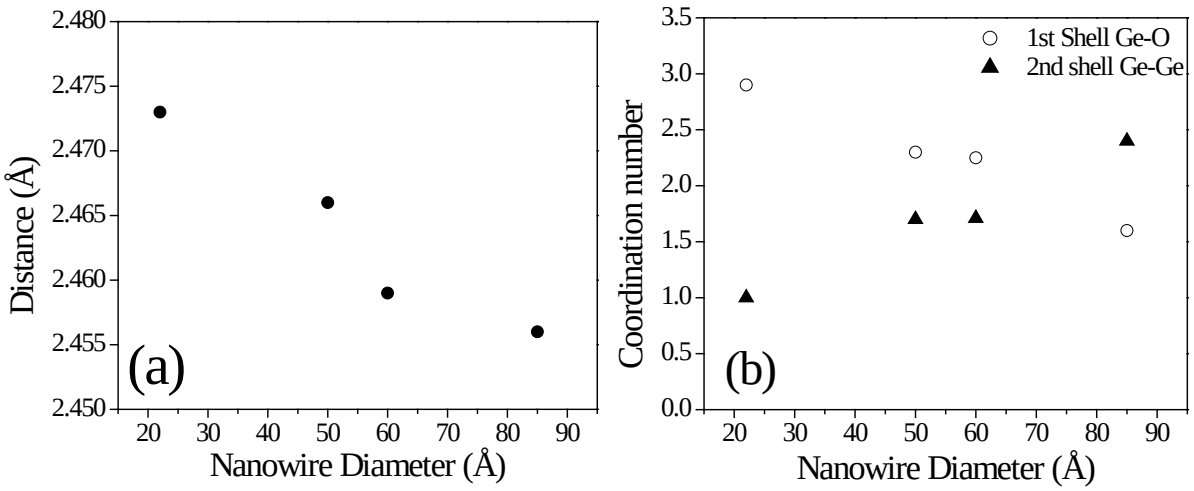

Figure 5 (a) Ge-Ge distance (second shell) in function of nanowires diameter. Distance corresponding to a tetrahedral environment. (b) Coordination number of the first 2 shells in function of nanowires diameter.

References

[1] T. Hanrath and B. A. Korgel, *Adv. Mater.*, 2003, **15**, 437.

[2] A. A. Yasseri, S. Sharma, T. I. Kamins, Z. Li, and R. S. Williams, *Appl. Phys. A.*, 2006, **82**, 659.

[3] S. Sharma, T. I. Kamins, and R. S. Williams, *Appl. Phys. A.*, 2005, **80**, 1225.

[4] T. Stelzner, G. Andra, E. Wendler, W. Wesch, R. Scholz, U. Goesele, and S. Christiansen, *Nanotechnology*, 2006, **17**, 2895.

[5] D. Wang, Y.-L. Chang, Z. Liu, and H. Dai, *J. Am. Chem. Soc.*, 2005, **127**, 11871.

[6] H. Adhikari, A. F. Marshall, C. E. D. Chidsey, and P. C. McIntyre, *Nano Lett.*, 2006, **6**, 318.

[7] S.-M. Liu, M. Kobayashi, S. Sato, and K. Kimura, *Chem. Commun.*, 2005, 4690.

[8] J. R. Heath and F. K. LeGoues, *Chem. Phys. Lett.*, 1993, **208**, 263.

[9] H. Omi and T. Ogino, *Appl. Phys. Lett.*, 1997, **71**, 2163.

[10] D. Erts, B. Polyakov, B. Daly, M. A. Morris, S. Ellingboe, J. Boland, and J. D. Holmes, *J. Phys. Chem. B*, 2006, **110**, 820.

[11] G. Audoit, E. N. Mhuircheartaigh, S. M. Lipson, M. A. Morris, W. J. Blau, and J. D. Holmes, *J. Mater. Chem.*, 2005, **15**, 4809.

[12] K. J. Ziegler, B. Polyakov, J. S. Kulkarni, T. A. Crowley, K. M. Ryan, M. A. Morris, D. Erts, and J. D. Holmes, *J. Mater. Chem.*, 2004, **14**, 585.

[13] T. A. Crowley, B. Daly, M. A. Morris, D. Erts, O. Kazakova, J. J. Boland, B. Wu, and J. D. Holmes, *J. Mater. Chem.*, 2005, **15**, 2408.

[14] T. Clifford, Oxford University Press, 1999.

[15] J. S. Kulkarni, O. Kazakova, D. Erts, M. A. Morris, M. T. Shaw, and J. D. Holmes, *Chem. Mater.*, 2005, **17**, 3615.

[16] O. Kazakova, D. Erts, T. A. Crowley, J. S. Kulkarni, and J. D. Holmes, *J. Magn. Magn. Mater.*, 2005, **286**, 171.

[17] K.-B. Lee, S.-M. Lee, and J. Cheon, *Adv. Mater.*, 2001, **13**, 517.

[18] P. Z. Pawlow, *Phys. Chem*, 1909, **65**, 545.

[19] T. Castro, R. Reifenberger, E. Choi, and R. P. Andres, *Phys. Rev. B.*, 1990, **42**, 8548.

[20] Z.-Y. Lu, C.-Z. Wang, and K.-M. Ho, *Phys. Rev. B.*, 2000, **61**, 2329.

[21] K. K. Nanda, S. N. Sahu, and S. N. Behera, *Phys. Rev. A.*, 2002, **66**, 013208/1.

[22] U. Tartaglino, T. Zykova-Timan, F. Ercolessi, and E. Tosatti, *Phys. Rep.*, 2005, **411**, 291.

[23] Z. Zhang, M. Zhao, and Q. Jiang, *Semicond. Sci. Tech.*, 2001, **16**, L33.

[24] L. Hui, F. Pederiva, B. L. Wang, J. L. Wang, and G. H. Wang, *Appl. Phys. Lett.*, 2005, **86**, 011913/1.

[25] L. Hui, B. L. Wang, J. L. Wang, and G. H. Wang, *J. Chem. Phys.*, 2004, **120**, 3431.

[26] B. Wang, G. Wang, X. Chen, and J. Zhao, *Phys. Rev. B.*, 2003, **67**, 193403/1.

[27] K. Dick, T. Dhanasekaran, Z. Zhang, and D. Meisel, *J. Am. Chem. Soc.*, 2002, **124**, 2312.

[28] M. Zhang, M. Y. Efremov, F. Schiettekatte, E. A. Olson, A. T. Kwan, S. L. Lai, T. Wisleder, J. E. Greene, and L. H. Allen, *Phys. Rev. B.*, 2000, **62**, 10548.

[29] S. L. Lai, J. Y. Guo, V. Petrova, G. Ramanath, and L. H. Allen, *Phys. Rev. Lett.*, 1996, **77**, 99.

[30] K.-S. Moon, H. Dong, R. Maric, S. Pothukuchi, A. Hunt, Y. Li, and C. P. Wong, *J. Electron. Mater.*, 2005, **34**, 168.

[31] Y. Wu and P. Yang, *Adv. Mater.*, 2001, **13**, 520.

[32] K. Lu and Z. H. Jin, *Curr. Opin. Solid St. M.*, 2001, **5**, 39.

[33] D. L. Zhang and B. Cantor, *Acta Metall. Mater.*, 1991, **39**, 1595.

[34] H. W. Sheng, G. Ren, L. M. Peng, Z. Q. Hu, and K. Lu, *J. Mater. Res.*, 1997, **12**, 119.

[35] L. Gråbaek, J. Bohr, E. Johnson, A. Johansen, L. Sarholt-Kristensen, and H. H. Andersen, *Phys. Rev. Lett.*, 1990, **64**, 934 LP

[36] R. Goswami and K. Chattopadhyay, *Phil. Mag. Lett.*, 1993, **68**, 215.

[37] J. Zhong, L. H. Zhang, Z. H. Jin, M. L. Sui, and K. Lu, *Acta Mater.*, 2001, **49**, 2897.

[38] X. W. Wang, G. T. Fei, K. Zheng, Z. Jin, and L. D. Zhang, *Appl. Phys. Lett.*, 2006, **88**, 173114.

[39] K. M. Ryan, N. R. B. Coleman, D. M. Lyons, J. P. Hanrahan, T. R. Spalding, M. A. Morris, D. C. Steytler, R. K. Heenan, and J. D. Holmes, *Langmuir*, 2002, **18**, 4996.

[40] N. R. B. Coleman, K. M. Ryan, T. R. Spalding, J. D. Holmes, and M. A. Morris, *Chem. Phys. Lett.*, 2001, **343**, 1.

[41] H. Lao and C. Detellier, Elsevier Sc. Ltd., 1996.

[42] N. Binsted, in 'EXCURV98: CCLRC Daresbury Laboratory computer program.' 1998.

[43] S. M. Sze, 'Physics of Semiconductor Devices', Wiley-Interscience, 1981.

[44] C. Q. Sun, Y. Wang, B. K. Tay, S. Li, H. Huang, and Y. B. Zhang, *J. Phys. Chem. B*, 2002, **106**, 10701.

[45] G. E. Brown, G. A. Parks, and P. A. O'Day, in 'Mineral Surfaces', ed. D. J. Vaughan and R. A. D. Patrick, London, 1993.